JGR Solid Earth

RESEARCH ARTICLE
10.1029/2019JB019203

Seismicity on Conjugate Faults in Ölfus, South Iceland: Case Study of the 1998 Hjalli-Ölfus Earthquake

R. M. Parameswaran[1], B. S. Thorbjarnardóttir[1], R. Stefánsson[2], and I. Th. Bjarnason[1,3]

[1]Institute of Earth Sciences, University of Iceland, Reykjavik, Iceland, [2]Faculty of Business and Science, University of Akureyri, Akureyri, Iceland, [3]Nordic Volcanological Center, Institute of Earth Sciences, University of Iceland, Reykjavik, Iceland

Key Points:
- Illustrates the spatiotemporal evolution of seismicity in Ölfus, the western segment of the South Iceland Seismic Zone (SISZ)
- Evaluates earthquake faulting mechanisms in Ölfus and compares them to the rest of SISZ
- Demostrates the interplay between conjugate faults during seismic sequences and dominance of seismic trend over ~N-S seismicity in Ölfus

Supporting Information:
- Supporting Information S1
- Movie S1
- Movie S2

Correspondence to:
R. M. Parameswaran,
revathy@hi.is

Citation:
Parameswaran, R. M., Thorbjarnardóttir, B. S., Stefánsson, R., & Bjarnason, I. T. (2020). Seismicity on conjugate faults in Ölfus, South Iceland: Case study of the 1998 Hjalli-Ölfus earthquake. *Journal of Geophysical Research: Solid Earth*, *125*, e2019JB019203. https://doi.org/10.1029/2019JB019203

Received 7 DEC 2019
Accepted 26 JUN 2020
Accepted article online 29 JUN 2020

Abstract The Ölfus seismic belt lies at the western end of the ~E-W sinistral transform shear zone in South Iceland, called the South Iceland Seismic Zone (SISZ), where most seismicity and surface faulting show ~N-S dextral slip. Unlike the rest of SISZ, seismicity in west Ölfus is predominantly along the ~ENE-WSW direction. Throughout recorded history, Ölfus has shown an interactive behavior with the Hengill volcanic system that lies northwest of the zone. For instance, the 13 November 1998 Mw 5.1 earthquake in the Hjalli area (west Ölfus) and its ~ENE trending aftershock sequence were likely triggered by the 4 June 1998 Mw 5.4 Hengill earthquake sequence. These events point to an interplay between conjugate ~N-S and ~ENE-WSW faults in the region. Relative relocations of earthquakes in Hjalli-Ölfus from July 1991 to December 1999 (Icelandic Meteorological Office, 2017) are chiefly limited to 4- to 8-km depth along the ~ENE direction with a few distributed on smaller ~N-S faults. The foreshocks of the November 1998 earthquake occurred on a ~N-S fault until a day prior to the mainshock when they shifted to the ~ENE direction. The subsequent aftershocks are also mainly restricted to the ~ENE direction. We find that the Mw 5.1 (Global Centroid Moment Tensor moment = 5.43×10^{16} N-m) Hjalli-Ölfus earthquake ruptured a near-vertical ~ENE fault area of 24–40 km^2 with left-lateral average slip of 5–8 cm. Multiple relocations of the mainshock using various constraints indicate that the event likely occurred close to the junction of the conjugate ~ENE-WSW and ~N-S faults.

1. Introduction

The sinistral South Iceland Seismic Zone (SISZ) and the transtensional oblique-spreading Reykjanes Peninsula (RP) accommodate the shift in plate divergence between the Eastern Volcanic Zone (EVZ) and the offshore Reykjanes Ridge in South Iceland (Einarsson et al., 1981; Taylor et al., 1994) (Figure 1a). The plate boundary along SISZ manifests as active microseismicity in an ~10- to 20-km-wide N-S and ~80-km-long E-W zone in the South Iceland Lowlands (SIL). It extends ~70 km further along RP to the west but trends ~ENE-WSW and tapers to ~5-km width at the western tip of the peninsula. A significant part of the sinistral transform motion on SISZ is accommodated by large earthquakes (Roth, 2004) on N-S dextral faults exhibiting "bookshelf-like" characteristic along the E-W trending SISZ (Einarsson et al., 1981). This zone is part of a larger region called the Hreppar formation that has older exposed bedrock north of SISZ exhibiting ENE trending sinistral and N-S to NNE trending dextral faults, with a few NE trending sinistral faults (Gudmundsson, 2017; Karson et al., 2018; Khodayar et al., 2020; Khodayar & Franzson, 2007). They have been mostly aseismic during recorded history with some exceptions (Thorbjarnardóttir et al., 2018). We find that recent ArcDEM images suggest major (~25 km), unmapped, ENE-WSW trending lineaments crossing the Hreppar formation (Porter et al., 2018; ArcDEM database). A similar pattern of faulting accompanies the plate divergence in RP (Erlendsson & Einarsson, 1996), with the larger earthquakes occurring on ~N-S dextral faults in the central and eastern parts of the peninsula (Björnsson et al., 2018).

The rupture length on corresponding N-S faults in SISZ has been estimated to be ≥20 km for large earthquakes (Bjarnason et al., 1993; Roth, 2004). Historically, significant destructive seismic sequences have been identified during 1630–1633, 1732–1734, 1784, and in 1896 when up to five intense events were recorded over a span of 2 weeks (Björnsson, 1976; Einarsson et al., 1981) (selected events in Figure 1b). Destruction areas in these sequences are documented to be elongated mostly in the ~N-S direction and some trending ~E-W (Björnsson, 1976; Einarsson et al., 1981). The largest event to occur in instrumentally recorded history in South Iceland is the 1912 M_s = 7.0 earthquake (Bjarnason, Cowie, et al., 1993; Gutenberg &

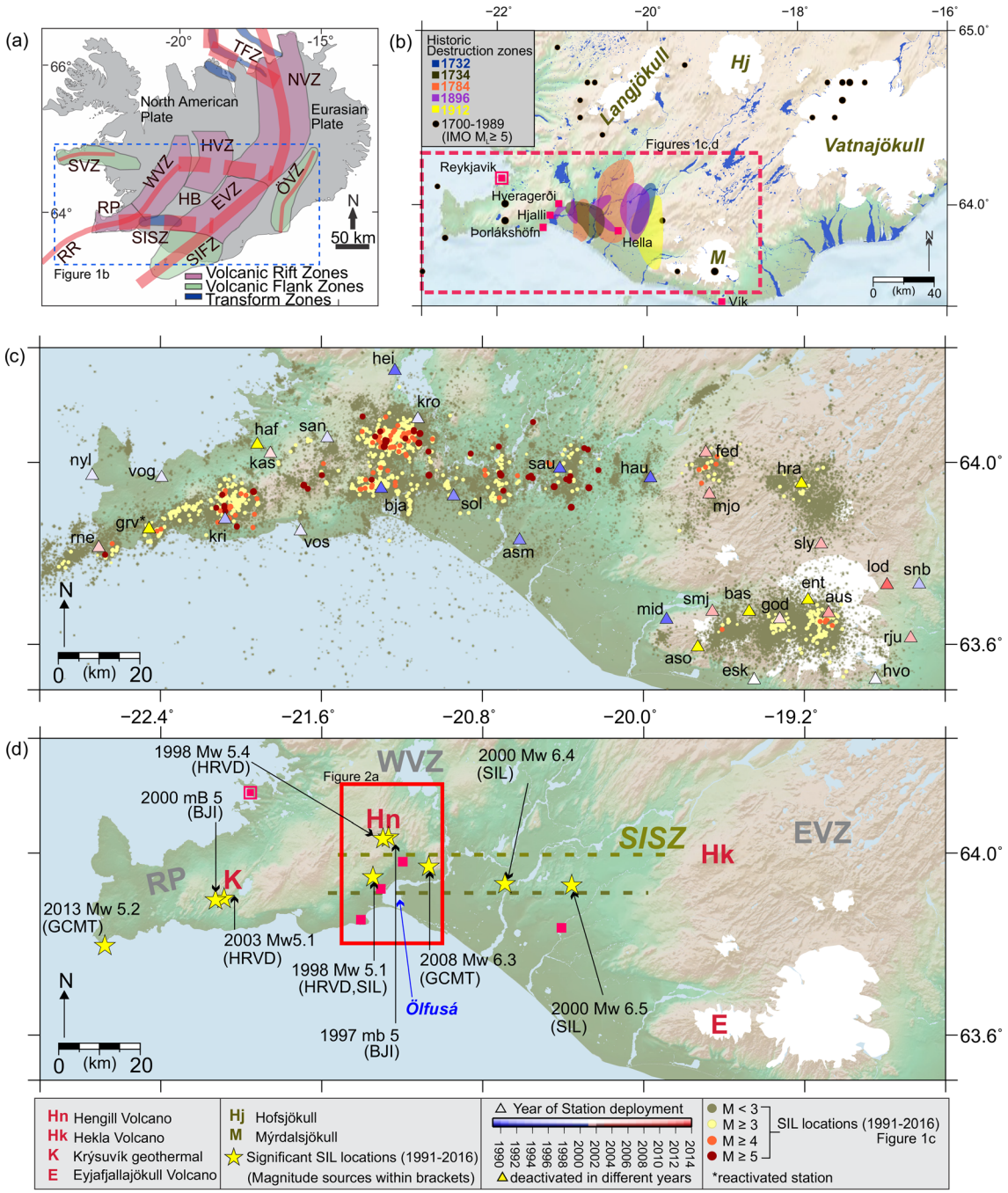

Figure 1. Seismicity in South-Southwest Iceland. (a) Salient tectonic and volcanic features in Iceland. TFZ = Tjörnes Fracture Zone; NVZ = Northern Volcanic Zone; EVZ = Eastern Volcanic Zone; ÖVZ = Öræfajökull Volcanic Zone; HVZ = Hofsjökull Volcanic Zone; WVZ = Western Volcanic Zone; SVZ = Snæfellsnes Volcanic Zone; RP = Reykjanes Peninsula; RR = Reykjanes Ridge; SISZ = South Iceland Seismic Zone; SIFZ = South Iceland Volcanic Flank Zone; HB = Hreppar Block (modified after Sigmundsson et al., 2018). (b) Historic context for seismicity in South Iceland. Observed destruction zones for historic earthquakes in the SISZ from 1732, 1734, 1784, 1896, and 1912 are indicated (Einarsson et al., 1981). Other $M_L \geq 5$ events between 1700 and 1989 are also marked (source: Icelandic Meteorological Office [IMO]). (c) Seismicity in South Iceland between 1991 and 2016, recorded by the South Iceland Lowlands (SIL) network that is mapped on the figure. (d) Significant $Mw \geq 5$ events in South Iceland including the 4 June 1998 Mw 5.4 Hengill and 13 November 1998 Mw 5.1 Ölfus earthquakes.

Richter, 1954). Based on the return periods of these events, a tentative quiet period of 45–112 years was assigned to this seismic zone (Einarsson & Björnsson, 1979), but an average of 140 years was estimated for complete stress release (seismic cycle) along SISZ (Stefánsson & Halldórsson, 1988). It has been argued

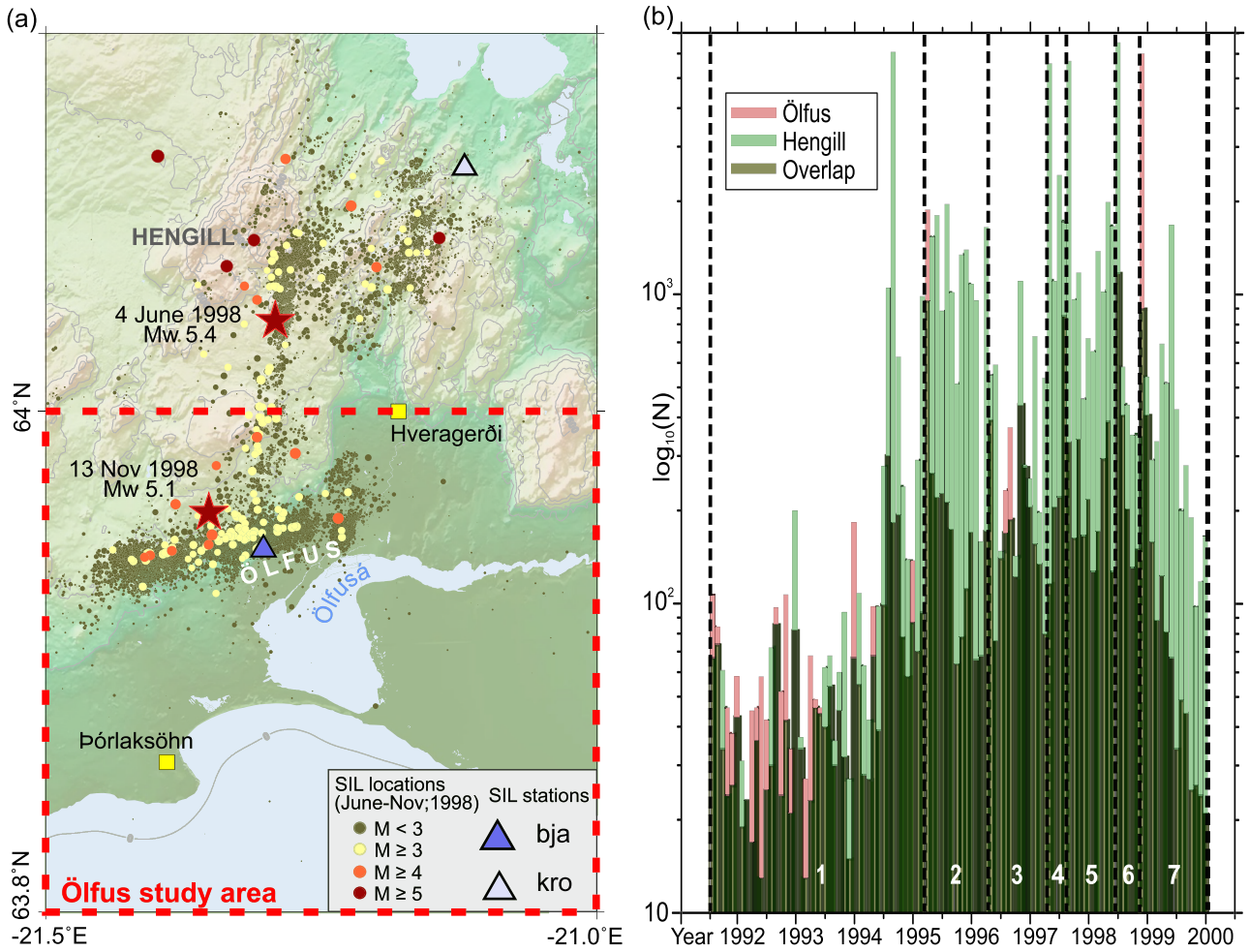

Figure 2. Definition of study area. Hengill-Ölfus seismic system. (a) Epicenter distribution of all recorded events in Hengill and Ölfus through the months of June 1998 to November 1998 (to see the seismic interaction view, refer to Movie S1). Red dashed square defines the Ölfus study area (b) Base-10 logarithmic plot of monthly seismicity in Ölfus versus Hengill from July 1991 to December 1999. Time windows (TW) are separated by black dashed lines and denoted by white numerals.

that part of the latest stress buildup since the 1896 and 1912 events in the eastern part of SISZ manifested as the 1987 Mw 5.9 (centroid moment magnitude) earthquake that occurred at the junction of SISZ and the western flank of EVZ, ~10 km east of the 1912 earthquake (Bjarnason & Einarsson, 1991). In more recent times, two large sequences of earthquakes in the Years 2000 (17 June Mw 6.5 and 21 June Mw 6.4) (Árnadóttir et al., 2001; Stefánsson et al., 2000) and 2008 (29 May; ~Mw 6.3 doublet in a span of 3 s) (Brandsdóttir et al., 2010; Hensch et al., 2016; Hreinsdóttir et al., 2009) have occurred on SISZ (Figure 1d), all on ~N-S faults (Clifton & Einarsson, 2005; Hjaltadóttir, 2009).

An exception to N-S faulting in SISZ is observed in its western part, in the municipality of Ölfus through which the river Ölfusá flows (Figures 1d and 2a). Located directly south of the Hengill central volcano, this region marks the transition of the plate boundary from RP to SISZ. The seismicity in Ölfus has a vivid ENE-WSW trend, contrary to the more prominent N-S faults in other parts of SISZ (Figure 1c). A notable example of this seismicity was following the 13 November 1998 Mw 5.1 earthquake (Global Centroid Moment Tensor [GCMT] catalog) (Rognvaldsson et al., 1998; Vogfjörd et al., 2005) that succeeded the 4 June 1998 Mw 5.4 (GCMT) Hengill event, the aftershocks of which propagated south toward Ölfus (Figures 1d and 2a).

The present study examines the seismicity in Ölfus from July 1991 to December 1999, including the 13 November 1998 earthquake. The purpose of this study is threefold: one, identify spatial and temporal

trends in Ölfus from 1991–1999 seismicity, which has never been done in detail, except a technical report of the November 1998 event by Rognvaldsson et al. (1998); two, consequently ascertain the depth and lateral extents of the Ölfus seismogenic zone; and three, develop a picture of seismic interaction between the conjugate faults (fault mechanics) in Ölfus and compare with published results on SISZ seismicity. This study is further explored in a subsequent paper on stress inversions performed on selected seismic activity.

1.1. Seismotectonic Background and Context

The divergence across the North American-Eurasian plate boundary in Iceland has been constrained to ~18–19 mm/year for the Eurasian plate with respect to the North American plate, along a velocity vector trending 104–105° (DeMets et al., 2010). In North Iceland, influence of the Icelandic hotspot on the plate boundary moves the divergence eastward toward the Northern Volcanic Zone through dextral transform faulting along the Tjörnes Fracture Zone (Figure 1a). In the south, the plate boundary regains its former trend through sinistral shear motion along SISZ and RP. In the southern half of Iceland, the net divergence is partitioned between EVZ and the Western Volcanic Zone (WVZ), the latter spreading at a reduced rate (one fifth to one third) compared to the former (Árnadóttir et al., 2008; LaFemina et al., 2005). LaFemina et al. (2005) estimates these spreading rates to be ~2–7 mm/year across WVZ, ~11–19 mm/year across EVZ, and ~14 mm/year along SISZ that connects the two volcanic zones. It has been suggested that the overlap spreading along WVZ and EVZ could temporarily isolate areas between them that could behave anomalous to the North American and the Eurasian plate motions (Karson, 2017). Such an independent block is believed to be bound by the EVZ, WVZ, SISZ, and the Höfsjökull Volcanic Zone in south central Iceland and is popularly referred to as the Hreppar block (HB)/microplate (Einarsson, 2008) (Figure 1a). The SW corner of the HB is commonly known as the Hengill Junction due to its proximity to the Hengill volcanic system. Foulger (1988) suggested that this region could be a triple junction between the transform-faulting SISZ, the rifting WVZ, and the transtensional RP.

RP is the aerial manifestation of the submerged Reykjanes Ridge, an oceanic segment of the MAR. The 70–80° trending plate boundary in RP is oblique to the plate motion direction (Árnadóttir et al., 2006; Brander et al., 1976; Einarsson, 1991), where divergence occurs along northeast-trending faults and fissures (Clifton & Schlische, 2003; Gudmundsson, 2017). The sinistral shear is accommodated by ductile deformation below a locking depth of 6 km (Hreinsdóttir et al., 2001) and along N to NNE-striking right-lateral strike-slip faults closer to the surface (Keiding et al., 2008; Khodayar et al., 2018). However, seismicity in the peninsula mostly manifests as normal-faulting seismic swarms along the rift in the west and as dextral earthquakes on the ~N-S faults in the east toward the SISZ (e.g., Árnadóttir et al., 2004; Keiding et al., 2009). The largest events in the region occur on these ~N-S features and have been known to reach magnitudes of M ~ 6.0 (Árnadóttir et al., 2004; Björnsson et al., 2018; Erlendsson & Einarsson, 1996) and show seismic correlation with the activity in WVZ and SISZ (Árnadóttir et al., 2004).

One indication of this is the seismic interaction between Ölfus and Hengill that has been observed numerous times in recorded history. For instance, the sequences from 1953–1955 (Ármannsdóttir, 2008; Tryggvason, 1954, 1956) and 1974–1987 (Einarsson et al., 1981; Einarsson & Björnsson, 1987) present evidence of interaction prior to the establishment of the SIL seismic network in 1990 (Stefánsson, et al.,1993). Additionally, Figure 2b depicts the interaction between Hengill and Ölfus from July 1991 to December 1999. The May 2008 Mw 6.3 (GCMT) earthquake doublet near Ölfus and Flói, the most recent significant earthquakes in SISZ, has also been linked to contraction in the Hengill area (Árnadóttir et al., 2018). Apart from this, SISZ has a history of fueling its own seismicity. For example, the faults that ruptured during the 2008 activity in east Ölfus are reported to have been statically loaded by the June 2000 earthquakes (Arnadóttir et al., 2003; Decriem et al., 2010; Hreinsdóttir et al., 2009). Therefore, the correlation between activities of different tectonic arms of the junction needs further investigation. One step toward this is to investigate the western part of SISZ, namely, west Ölfus, and, thus, is the focus of the present study. Across its length, this municipality extends 5–40 km parallel to the river Ölfusá in the E-W direction. Western Ölfus is tectonically active on conjugate ENE-WSW and N-S faults, while eastern and central Ölfus experience earthquakes on N-S faults (e.g., 2008 sequence). Significant earthquakes in the early instrumentation period include the 9 October 1935 M6.0 earthquake in South Hengill near Hveradalir geothermal area (Halldórsson et al., 2013) and $M_L \leq 5.5$ events in 1955, relocated with an intensity study ~5–6 km north of Hjalli and west of town Hveragerdi (Ármannsdóttir, 2008). These events caused minor damage in the

Hjalli area and Hveragerdi (Ármannsdóttir, 2008; Halldórsson et al., 2013). The church farm at Hjalli in west Ölfus collapsed a minimum of six times prior to the Year 1789 over a period of four centuries (Halldórsson et al., 2013). The largest earthquake to occur in the Hjalli area was the 13 November 1998 Mw 5.1 earthquake (henceforth called the Hjalli-Ölfus earthquake), following the 4 June 1998 Mw 5.4 earthquake in Hengill. The Hengill earthquake cannot be associated with any significant earthquake along SISZ and was likely related to the 1994–1995 inflation episode in Hengill during the crustal deformation period of 1993–1998 (Feigl et al., 2000; Sigmundsson et al., 1997). Therefore, activity in western and central parts of Ölfus can be triggered by both Hengill and SISZ, thereby facilitating failure on ~ENE-WSW and ~N-S conjugate fault systems. The Ölfus seismicity has been continuously recorded by the Icelandic Meteorological Office seismic network (initially established as the SIL network) from 1991 to present (e.g., Jakobsdóttir, 2008; Stefánsson, 2011) and provides considerable scope for seismic analysis.

2. Data

We define the Ölfus study area within 63.8–64°N and 21.0–21.5°W, south of the Hengill volcanic system (Figures 2a). For the prescribed area, earthquake data from July 1991 to December 1999 were procured from the Icelandic Meteorological Office (2017). There are 22,354 earthquakes in the Ölfus region within the selected time interval in the Icelandic Meteorological Office catalog. Figure 2b documents the comparison between seismic swarm activities in Ölfus and Hengill for the defined time period. The data set is partitioned into time windows (TWs) based on spikes in seismic activity in Ölfus: (1) July 1991 to February 1995 (3,086 earthquakes), (2) March 1995 to March 1996 (3,699 earthquakes), (3) April 1996 to March 1997 (2,623 earthquakes), (4) April 1997 to July 1997 (1,396 earthquakes), (5) August 1997 to May 1998 (2,335 earthquakes), (6) June 1998 to October 1998 (2,057 earthquakes), and (7) November 1998 to December 1999 (7,158 earthquakes) (Figure 2b).

Our analysis of the SIL earthquake catalog shows that ~30% of earthquakes in South Iceland have an absolute location error within ±1.0 km. The lateral errors in longitude and latitude are usually within half of the error in depth, with longitude better constrained. Due to proximity of the nearest SIL station (BJA) to the Hjalli seismicity, a higher portion of these events have absolute location errors within ±1.0 km (Figure 4). The relocation method used in our analysis (next section) further selects the most consistent phase data (good quality), which tends to be over 54% of the total Hjalli sequence from July 1991 to December 1999. Of the selected subsets for relocation, approximately half have absolute location error within ±1.0 km.

3. Methodology

The events from each TW are relatively relocated using the double difference inversion routine by Waldhauser and Ellsworth (2000) (see also Waldhauser, 2001). The method involves minimizing the residual time between observed and calculated differential traveltimes between a pair of earthquakes (ij) observed at a station (k), defined as

$$dr_k^{ij} = \left(t_k^i - t_k^j\right)^{\text{obs}} - \left(t_k^i - t_k^j\right)^{\text{cal}} = \frac{\partial t_k^i}{\partial \mathbf{m}} \Delta \mathbf{m}^i - \frac{\partial t_k^j}{\partial \mathbf{m}} \Delta \mathbf{m}^j, \quad (1)$$

for earthquake pairs sufficiently close together. $\Delta\mathbf{m}$ is the perturbation (change) in the corresponding four relative hypocentral parameters (Δx, Δy, Δz, Δt) between a pair of earthquakes observed at station k. $t_k^i - t_k^j$ is the differential time between the pair, and dr_k^{ij} is the residual between observed and calculated differential times (double difference). The equation may either use absolute traveltimes of pick phases or cross-correlation of the waveforms of the earthquake pair that usually gives higher accuracy of relative traveltime difference. The present study employs the former method. A system of linear equations for the hypocentral pairs is set up from the data collected from all active stations, within a certain epicentral distance. This system of equations can be represented as

$$\mathbf{WGm} = \mathbf{Wd}, \quad (2)$$

where $\mathbf{G}$ is the partial derivative matrix of size Mx$4N$, $\mathbf{m}$ is a column vector of length $4N$ containing hypocentral perturbations, $\mathbf{d}$ is the double-difference data vector of length M, and $\mathbf{W}$ is the diagonal weighting matrix. A damping factor can be introduced to ensure stability of the solution, such that

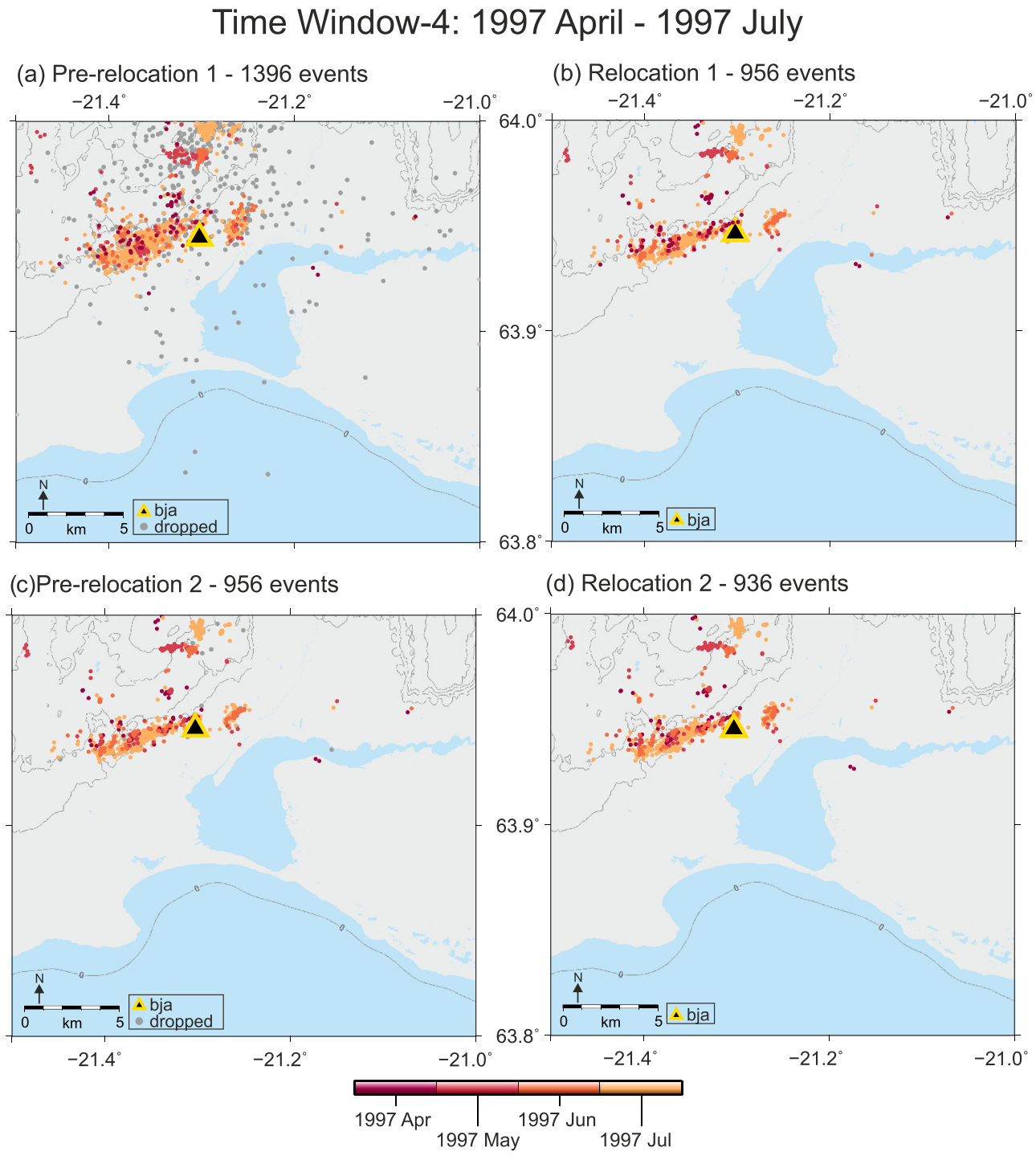

Figure 3. Relative relocations for TW-4 (1997 April to 1997 July). (a) Raw SIL locations for TW-4. Colored events were selected for relocation. Dropped events stand for events dropped by the double-difference routine and are indicated as gray circles. (b) Relatively relocated events from the first round of inversion. (c) Results from (b) subjected for a second round of relative relocations. (d) Final set of relatively relocated events for TW-4.

$$\mathbf{W}\begin{bmatrix}\mathbf{G}\\ \lambda\mathbf{I}\end{bmatrix}\mathbf{m} = \mathbf{W}\begin{bmatrix}\mathbf{d}\\ \mathbf{0}\end{bmatrix}. \tag{3}$$

Equation 3 can now be solved for $\mathbf{m}$ by either single value decomposition (SVD) or the iterative least squares method. For large numbers of events within a cluster, least squares estimates are

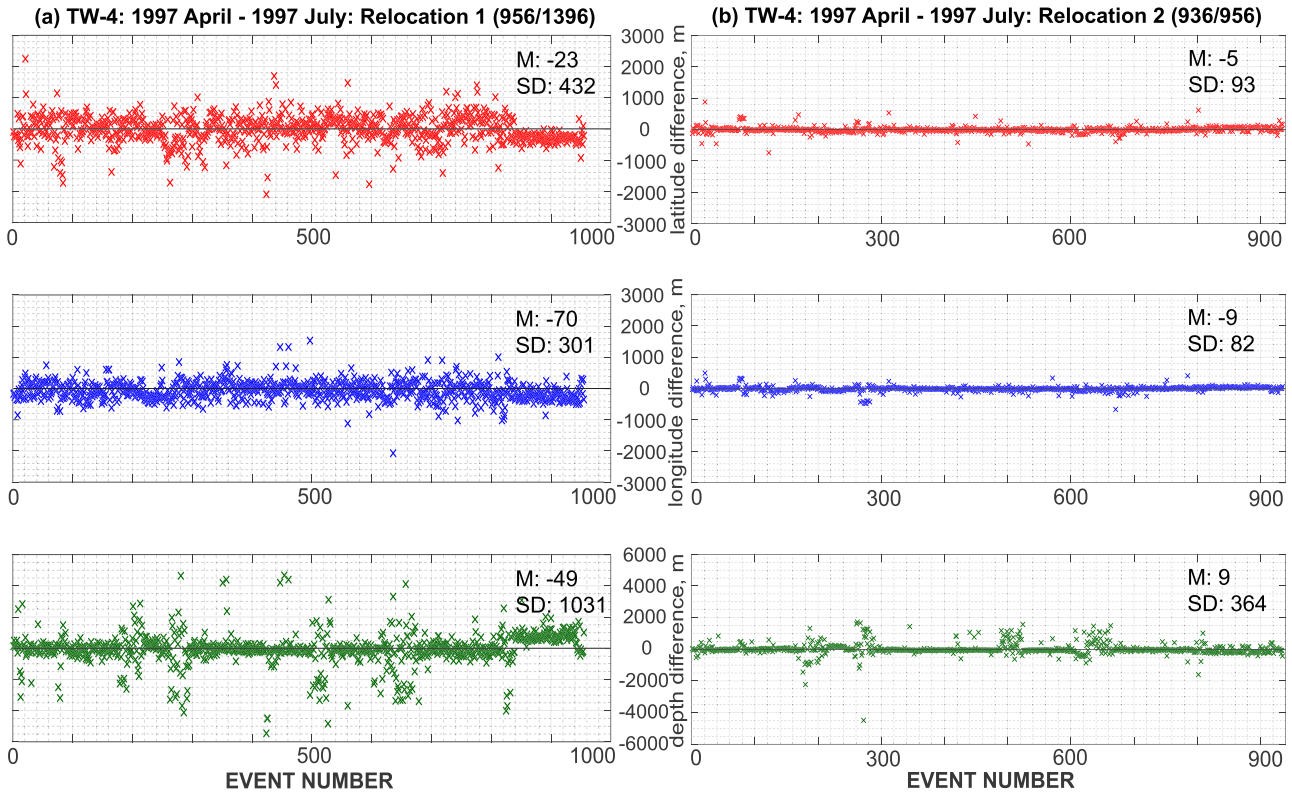

Figure 4. Shifts in hypocentral parameters. Example of mean (*M*) and standard deviations (*SD*) for change (in meters) in latitude, longitude, and depth for TW-4: (a) Relocation 1 and (b) Relocation 2.

computationally less intensive and is the chosen method of relocation in this study. However, for reliable error analysis, SVD inversion was applied (Waldhauser & Ellsworth, 2000) to a subset of the data within TW4 (see Supporting Information S1).

The number of active stations used in each TW varies as the SIL network was being expanded and altered in the 1990s. The years of deployment are indicated in Figure 1. The original SIL data from 1991–1999 were acquired using the 1-D SIL velocity model with constant velocity gradient in each layer (Stefánsson et al., 1993), based on refraction profiles in South and West Iceland (Bjarnason et al., 1993). The current study uses a constant velocity layer version of the SIL model, with twice as many layers as the gradient version. Event pairs in each TW are subjected to two rounds of relative relocations to verify the stability of convergence. Since the SIL seismic network was in its infancy from 1991 to 1994, TW-1 potentially has higher absolute and relative location errors arising from limited station coverage (Figure S1). Relocation results from other TWs and their statistics can be found in Figures 3, 4, and S2–S6. Figures 3 and 4 illustrate the two-stage relative relocation for TW-4. During the first stage of relocations for this TW, the double-difference routine relocates 956 earthquakes out of the 1,396 events located by the network (Figures 3a and 3b). The corresponding changes in the hypocentral spatial parameters are plotted in Figure 4a, where the mean and standard deviations are given in meters. The second round of relative relocations selects 936 earthquakes out of the 956 relocated events from the first round (Figures 3c and 3d). The SVD error analysis for TW-4 is detailed in Figure S7. The relocated events from each TW are overlain on identified/proposed fault/fracture systems compiled by Steigerwald et al. (2018) in the study area (Figure 5). It is to be noted that the fractures mapped here probably do not show all the fault sets and traces present in the area. For instance, Khodayar et al. (2020) finds that 23% of fractures in HB and SISZ strike NNE, while 77% are primarily ~N dextral and ENE sinistral and secondarily E-W, WNW, and NW sinistral strike- and oblique-slip structures, forming a leaky transform zone.

To examine the depth distribution of relocated events, projections (orthographic) are also constructed for relocated events from TW-2 to TW-7 on planes tilted 1° (toward observer) from the vertical. The azimuths

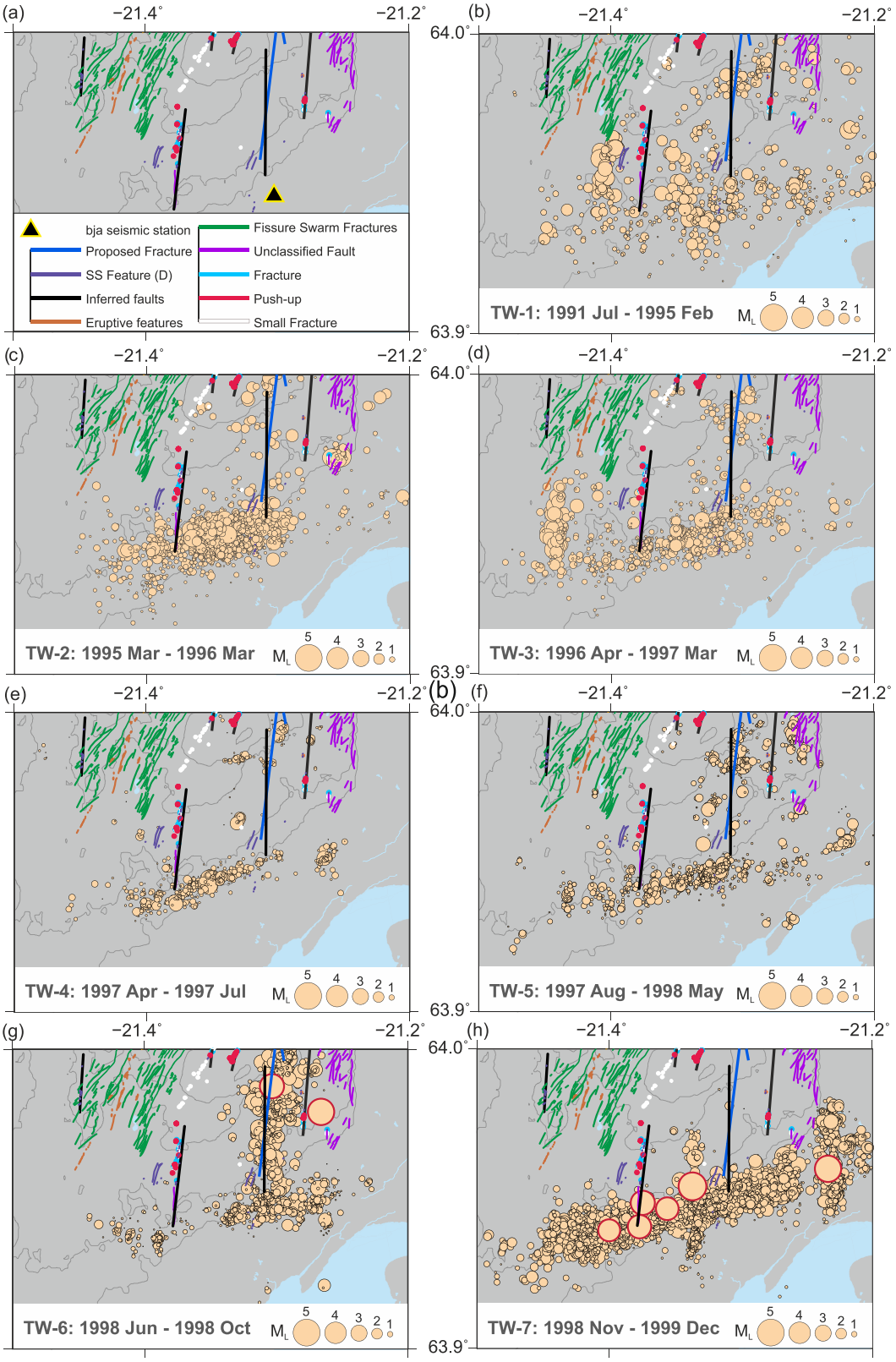

Figure 5. Correlation between Ölfus seismicity and surface features. (a) Surficial features and classifications identified by Steigerwald et al. (2018). Relocated seismicity from (b) TW-1, (c) TW-2, (d) TW-3, (e) TW-4, (f) TW-5, (g) TW-6, and (h) TW-7. Events encircled in red have $M_L \geq 4$ (SIL catalog).

of the projection planes are chosen in two directions: one perpendicular to the ~ENE-WSW seismicity and the other parallel, namely, the NNW-SSE and the ENE-WSW projection planes (henceforth called, AA′ and BB′ projections, respectively) (Figures 6–8). In TW-7, the aftershock sequence of the Mw 5.1 event on 13 November 1998 is examined in two ways over the backdrop of 6 days' worth of foreshock activity: (1) hourly seismicity for the first 10 hr postmainshock, followed by seismicity until the end of the day, with subsequent activity until the largest aftershock/triggered event, and finally the seismicity until the end of 48 hr postmainshock (Figure 8a and Movie S2); (2) daily seismicity for 7 days postmainshock (Figure 8b and Movie S2). Finally, to better interpret the fault movement during the November 1998 earthquake sequence, focal mechanisms of the foreshocks and aftershocks are analyzed in Figure 9.

4. Results

The first relocation reveals a considerable shift in hypocenter locations for earthquakes selected by the double-difference routine. For instance, the standard deviations of changes in latitude, longitude, and depth from their mean values for the first stage of relocations in TW-4 are 432, 301, and 1,031 m, respectively, although the mean value (centroid) shifts are moderate ($\leq$70 m). The second round of relative relocations confirmed good convergence for all TWs, where the centroid of each sequence moved <70 m (Figures S1–S6) and yielded lower values of mean and standard deviations compared to the first round (Figures 4a vs. 4b). It shows that the relative error tends to be an order of magnitude less than the absolute catalog location error or uncertainty within 100 m for this subset of the data (Figure S7). For larger subsets of the data, this estimate may, however, be an underestimate. The standard deviations of location differences between the first and second round of relocations may be an indication of the relative error of larger subsets (Figures S3–S6) and are usually within 200 m. Bjarnason and Thorbjarnardóttir (2019) carried out similar error analysis of SIL data throughout South Iceland and concluded that relative error is usually within an order of magnitude laterally and half an order of magnitude along depth, compared to the average error of single event locations.

The resultant set of relocated events does not align with most of the documented faults/fractures in Ölfus (Figure 5). A notable exception is the aftershock sequence of the 4 June 1998 Mw 5.4 Hengill earthquake that aligned with inferred/proposed faults/fractures (blue and black lines) extending all the way south to the west Ölfus seismic zone (TW-6; Figure 5g). Other minor clusters of seismic activity from TW-1 to TW-5, before the 1998 Hengill earthquake, also seem proximal to the same inferred/proposed fault/fracture (Figures 5b–5f). A few additional small clusters can be traced to certain unclassified faults (purple lines) in TW-1, TW-2, and TW-5 (Figures 5b, 5c, and 5f). Based on the epicentral distribution of the relocated events, an ~ENE-WSW seismic trend is prominent in all TWs, with some N-S trending activity stitching across it.

For TW-2, the AA′ and BB′ projections show the distribution of the relocated events from March 1995 to March 1996 (Figure 6a). The seismic swarm activity in this TW picks up in March 1995 and mostly spans the ENE-WSW direction. There seems to be some contemporaneous shallow seismic activity on unclassified faults (Figures 5 and 6a). However, the bulk of the seismicity, both in terms of number and larger magnitudes, is in the ~4- to 7-km depth range trending ENE.

Subsequently, TW-3 does not record any large swarm event but a generally higher activity than the baseline seismicity from previous years in Ölfus (Figures 2b and 6b). However, the depth projections and the epicentral plots display a notable ~N-S directed earthquake cluster at 4- to 5-km depth in April 1996, which does not correspond to any identified fault/fracture (Figures 5 and 6b). A smaller cluster at 7- to 8-km depth seems to occur in September 1996, directly below the April sequence (Figure 6b). Aside from these clusters, most of the hypocenters are restricted to the ENE trend. However, the magnitudes of events in the ENE-WSW direction are considerably smaller (mostly local moment magnitude Mlw < 2; few $\geq$ Mlw 2) than in the April 1996 cluster where several Mlw 2 and 3 earthquakes aligned along the N-S direction.

In April 1997, seismic activity in the Ölfus belt heightened, culminating in a small earthquake swarm in July 1997 (TW-4) (Figure 6c). Both depth projections and epicenter maps point to the same ENE trend, predominantly in the depth range 4 to 7 km. The ENE trend arises from a collection of hypocenters restricted to this direction. The distribution of the hypocenters in the AA′ projection suggests a near-vertical fault, dipping slightly NNW (Figure 6c(c2)). The proposed/inferred faults/fractures north of the Hjalli area show disjointed clusters of seismicity in TW-4 (Figures 5 and 6c). The ensuing seismicity from August 1997 to May 1998

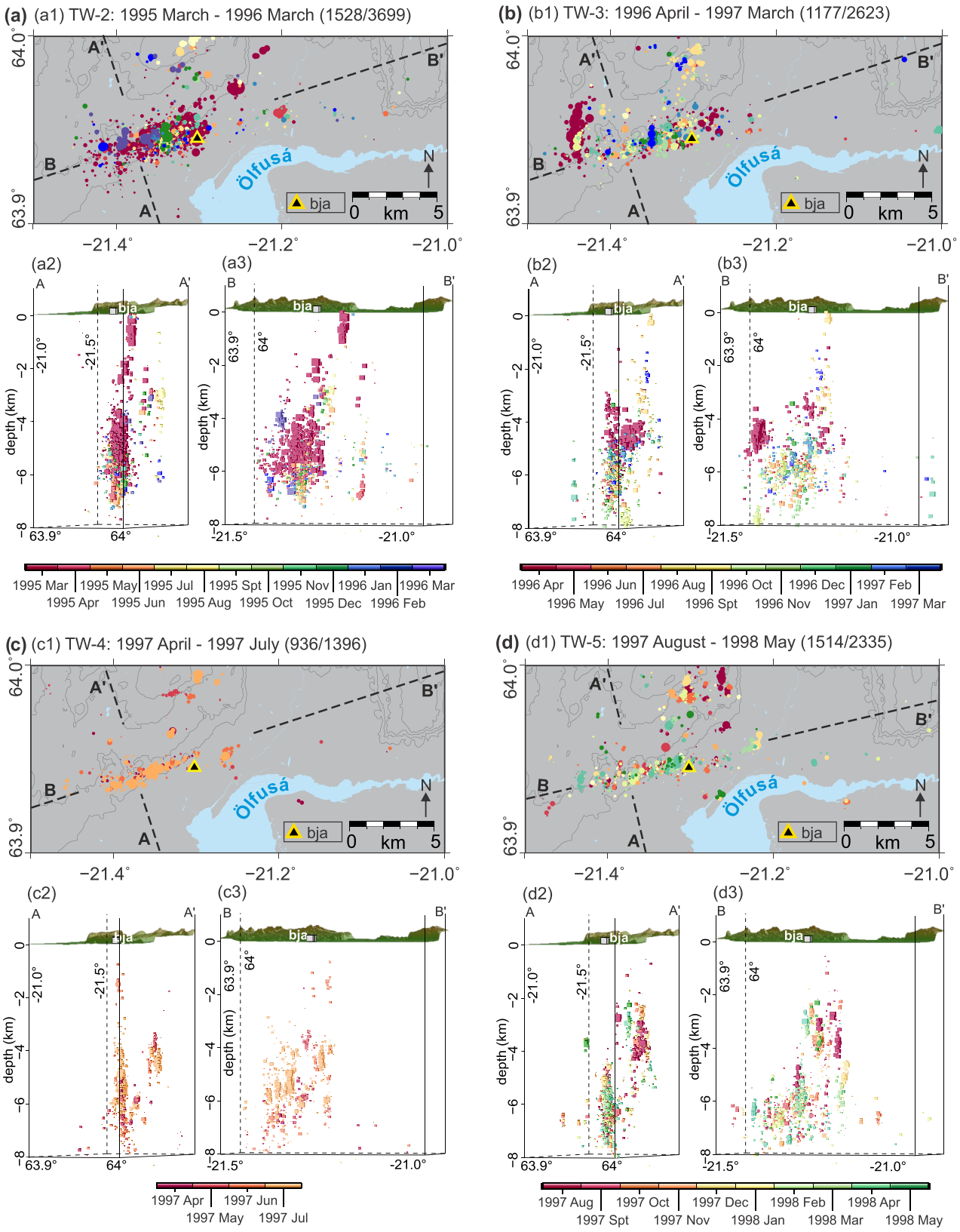

Figure 6. ENE and NNW projection profiles. (a) TW-2. (a1) Epicenter map of seismicity. Projections along (a2) AA′ and (a3) BB′. (b) TW-3. (b1) Epicenter map of seismicity. Projections along (b2) AA′ and (b3) BB′. (c) TW-4. (c1) Epicenter map of seismicity. Projections along (c2) AA′ and (c3) BB′. (d) TW-5. (d1) Epicenter map of seismicity. Projections along (d2) AA′ and (d3) BB′.

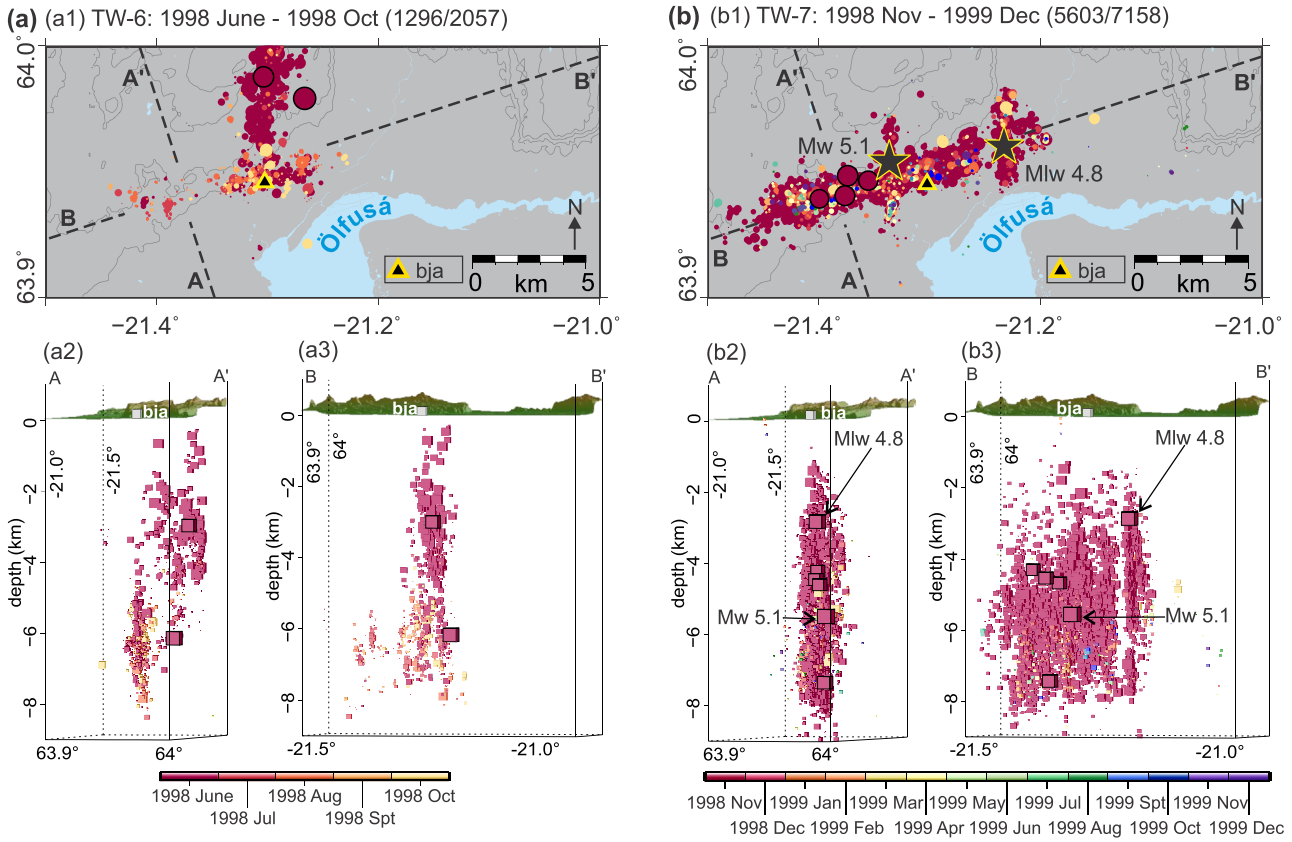

Figure 7. ENE and NNW projection profiles. (a) TW-6. (a1) Epicenter map of seismicity. Projections along (a2) AA′ and (a3) BB′. (b) TW-7. (b1) Epicenter map of seismicity. Projections along (b2) AA′ and (b3) BB′.

(TW-5) continues to exhibit a similar ENE pattern extending deeper (within 8 km) (Figure 6d). The exceptions to the ~ENE trend in TW-5 are a collection of epicenters parallel to the ~N-S-inferred/proposed faults in the north and an ~N-S array of epicenters to the west of the ~ENE-WSW Hjalli zone.

In TW-6, we observe aftershocks from the 4 June 1998 Hengill earthquake migrating south toward the Hjalli seismic zone (Figure 7a), between 4 and 17 June 1998. These earthquakes align with the inferred/proposed faults suggested by Steigerwald et al. (2018) (Figure 5). Among these earthquakes from the Hengill sequence are two M > 4 events at ~3- and ~6-km depths. However, it is noteworthy that most of the hypocenters in the ~N-S trend are rather shallow (2–5 km) (Figures 7a). The corresponding spread of hypocenters in the Hjalli area is restricted to 4- to 8-km depth, trending ~4 km long in the ENE-WSW direction at the southern terminus of the Hengill sequence.

In November 1998, the highest stress release over the discussed 4-year-long Hjalli seismic sequence occurred with a Mw 5.1 earthquake on the thirteenth of the month following the seismic activity in Hengill (TW-7; Figure 7b). During this TW, the most pronounced activity is again ENE-WSW, with a majority (~84%) of the relocated earthquakes occurring in November 1998 and 16% in the following months. The epicenter map and depth projections show two N-S seismic lineaments across the ENE-WSW trend (Figure 7b), the second one at the eastern end of the Hjalli area seismicity. However, neither of these N-S trending arrays of epicenters correlate to inferred/proposed faults (Figure 5h). The sources of the mainshock and the largest aftershock offset from the eastern end of the ENE-WSW seismicity align with these N-S seismic trends, but the remaining four Mlw > 4.0 events occur along the ENE-WSW direction. However, it is to be noted that the source of the mainshock lies close to the intersection of the ENE-WSW and N-S seismicity. Thus, the mainshock was relocated multiple times using either foreshocks/aftershocks or both from selected time frames to evaluate its relative position in these event combinations. It was further relocated after neglecting stations

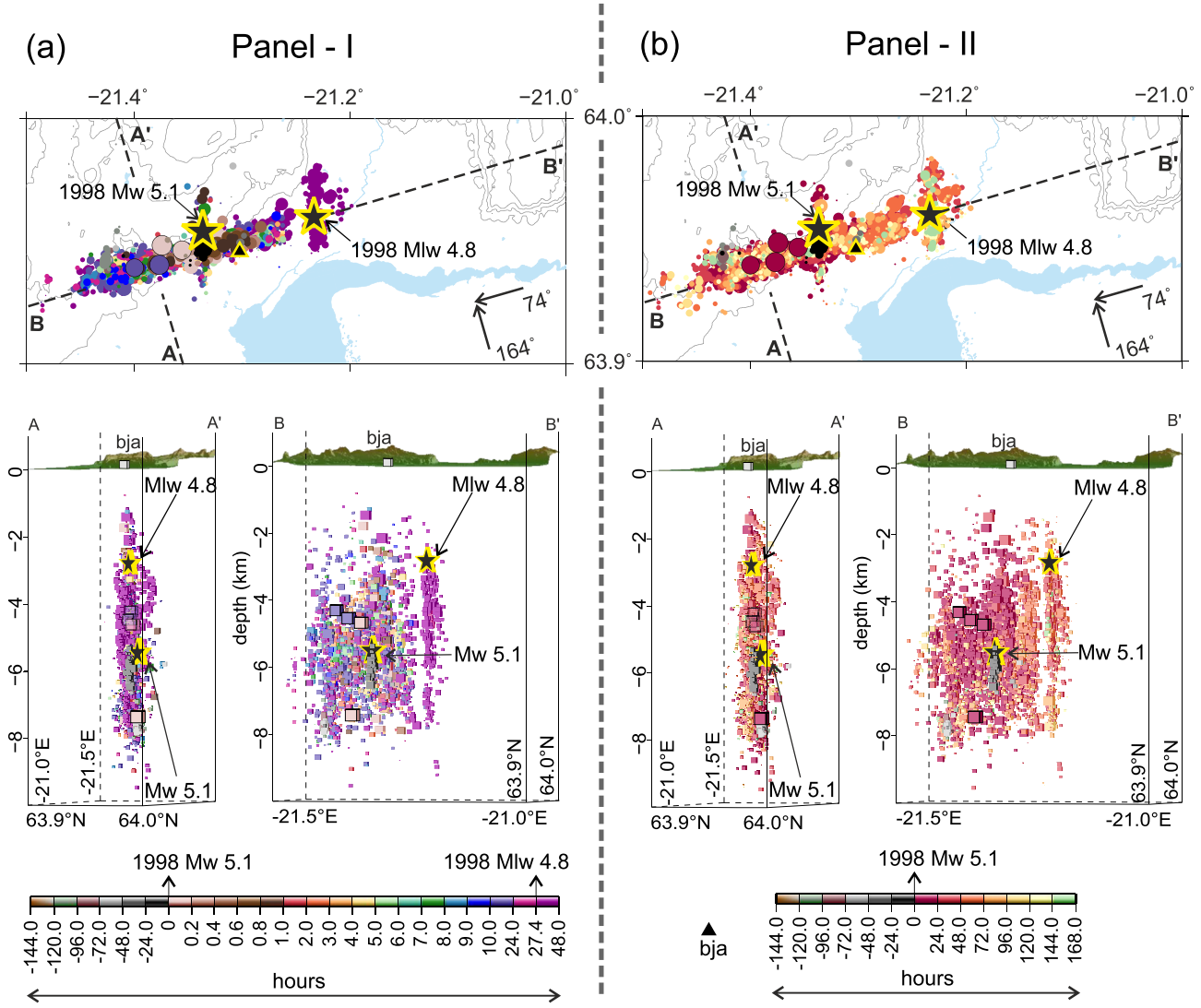

Figure 8. Spatiotemporal evolution of the 13 November 1998 seismic swarm in Ölfus. Epicenter maps and AA′ and BB′ projections of (a) Panel I: 6-day foreshock and 2-day aftershock seismicity (in hours). (b) Panel II: 6-day foreshock and 7-day aftershock seismicity (in hours).

which did not have an active time lock at the time of recording. These tests are further elaborated in Table S1 and locations displayed in Figure 9d.

The 6-day foreshock activity proximal to the nucleation of the mainshock, including four events with 3 > Mlw > 2.5, occurs between 5.5- and 6.5-km depth near the central N-S seismic trend (see Movie S2) However, only ~18% of aftershocks in the first hour occur along the N-S direction, while ~82%, including a Mlw 4.4 and a Mlw 4.2, occur along the ENE-WSW direction (Figure 8a, Panel I). Please note that the percentage of events attributed to the ~N-S direction is an overestimate as it includes events at the intersection of the conjugate faults. Therefore, the percentage assigned to the ENE-WSW direction is a conservative estimate. Over the next 6 hr, seismicity continues to occur in the ENE-WSW direction, with few to none of the relocated events falling on the central N-S trend. From Hours 8 to 27.4 after the mainshock, activity continues along the ENE-WSW direction, with some activity picking up on the central N-S fault. Within this span, two more 5 > Mlw > 4 events occurred on the ENE-WSW fault (Hours 10 to 24 after the mainshock) (Figure 8a and Movie S2). The potentially triggered Mlw 4.8 event on the eastern N-S fault occurred on 14 November 1998, 27.4 hr after the mainshock. This disjointed N-S trend of seismicity is offset by <1 km from the eastern terminus of the erstwhile aftershock activity of the 13 November mainshock.

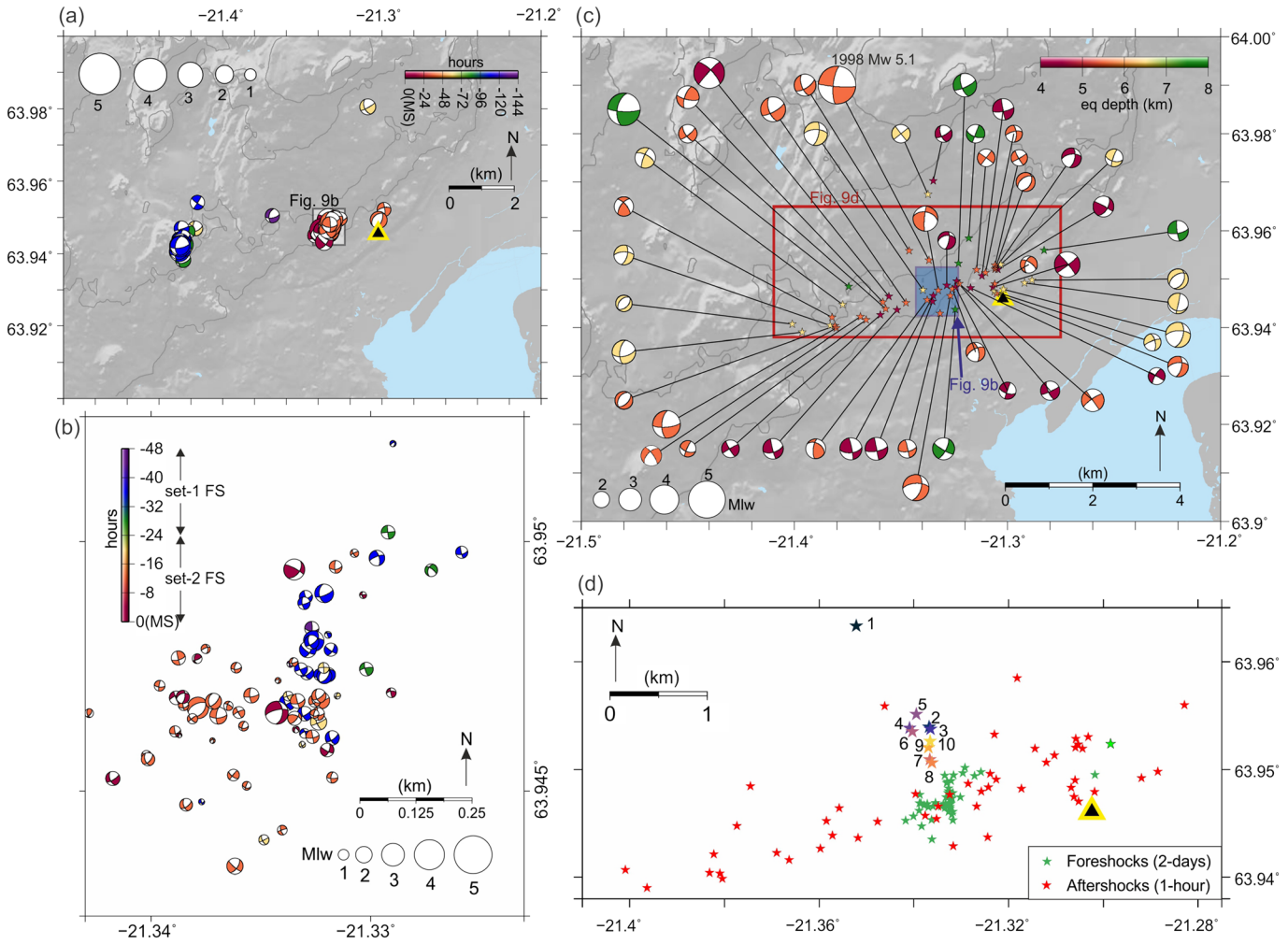

Figure 9. Focal mechanisms of foreshocks and aftershocks of 1998 Ölfus event. (a) Foreshocks 6 days prior to the mainshock, (b) foreshocks 2 days prior to mainshock, (c) aftershocks 1 hr after the mainshock, and (d) mainshock relocations using different sets of seismic stations and with respect to either foreshocks (2 days)/aftershocks (1 hr) or both (see Table S1). The numbers adjacent to the multicolored stars are listed in Table S1. The black triangle denotes station BJA.

The record of aftershocks indicates that ~88% of the seismicity, including four 5 > Mlw > 4 events in the first 24 hr, occurred along the ENE-WSW trend and the remaining ~12% on the central N-S lineament (Figure 8b, Panel II). As in the first hour of aftershocks, the percentage attributed to the ENE-WSW direction is a lower limit. In the following 24 hr (Day 2), the Mlw 4.8 event occurred ~5 km east of the mainshock on a separate N-S fault. Days 3–7 continue to show activity on all three conjugate faults, with ~69% of events on the ENE-WSW feature, ~5% on the central N-S fault, and ~26% on the eastern N-S fault. The seismicity spans between 2- and 10-km depth, with the highest concentration of hypocenters between 4- and 8-km depth. Foreshock and aftershock distributions of the Mw 5.1 Hjalli-Ölfus earthquake show contrasting trends. The foreshocks between 24 and 48 hr (Set 1) before the mainshock align in the N-S direction, while those within 24 hr prior to the main event (Set 2) trend in the ~ENE-WSW direction (Figures 9a and 9b). The focal mechanisms of these foreshocks (<48 hr before mainshock; Mlw > 0) are largely oblique normal and normal, with a few strike-slip. These fault-planes fit the observed active ~N-S and ~ENE-WSW conjugate seismic trends with dextral and sinistral slip, respectively. The first hour of aftershocks (Mlw ≥ 2) following the 13 November earthquake occur along the ~ENE-WSW direction, like the Set 2 foreshocks (Figure 9c). The focal mechanisms of these events are largely strike-slip, with a few oblique normal. The aftershocks likely occurred in the ~ENE-WSW direction, since nearly all of them align along this trend with sinistral slip. The Mlw < 2 events also align in the ENE-WSW direction within this hour but are left out in Figure 9c to

preserve its clarity. The locations of these events can be found in the Open Science Framework link listed in the Data Availability section at the end of this article. This analysis indicates that although an ~N-S fault may have been active 24 hr prior to the mainshock, we interpret that the event itself ruptured along the ~ENE-WSW fault, discussed in detail in the following section.

5. Discussion

5.1. Seismicity and Faulting in South Iceland

The general consensus about faulting in South Iceland is that the collection of seismically active ~N-S dextral faults cutting across the primary E-W trend of SISZ is young (Angelier et al., 2004; Bjarnason, Cowie, et al., 1993; Björnsson, 1976; Einarsson et al., 1981; Einarsson & Eiríksson, 1982; Gudmundsson & Brynjolfsson, 1993: Gudmundsson, 2007; Khodayar & Franzson, 2007; Tryggvason, 1973). Angelier et al. (2004) and Bergerat and Angelier (2008) suggest that the young strike-slip faulting in South Iceland can be explained in terms of Riedel shear fractures, observed in analog experiments, for a less-developed SISZ fracture system compared to the Hreppar formation north of it. However, the near-perpendicular angle of the ~N-S faults to the trend of the SISZ does not quite fit the fracture angle distribution observed in analog experiments (e.g., Davis et al., 2000). Gudmundsson (2007) proposed a structural strength barrier of the Hreppar anticline for a throughgoing ~E-W rupture in the SISZ rather than a general strength anisotropy of the crust (Bjarnason, Cowie, et al., 1993). The fault pattern in the Hreppar formation is similar to strike-slip faulting in the RP (Gudmundsson, 2017; Karson, 2017; Karson et al., 2018, 2019), where the Riedel shear analogy fits well (Clifton & Schlische, 2003; Khodayar et al., 2018). Detailed mapping of the destruction zones marked by damage to housing during the 6 September 1896 earthquake, extending between SISZ and Hreppar, indicates ESE-WNW as well as ~N-S destruction (Figure 3 in Björnsson, 1976). Significant sinistral faults in the SISZ may therefore still be largely hidden. They are possibly stronger- and/or less-developed faults and are activated only in large South Iceland earthquakes. Evidently, the western part of the SISZ in Ölfus has this great variety of faulting as observed on RP and HB. It may indicate a stress regime similar to the present RP and perhaps to Hreppar in the past, with activation along a major ~ENE-WSW fault and a conjugate array of N-S faults across the zone.

5.2. Hjalli-Ölfus Seismicity

The present study elucidates the predominance of an ~ENE-WSW rupture in Hjalli-Ölfus compared to the antithetic N-S ruptures dominant in SISZ. Relative relocations indicate that the Hjalli-Ölfus seismicity forms a tight, narrow, near-vertical array of hypocenters approximating a planar surface (henceforth called a plane) on the AA′ projections in all TWs (Figures 6a(a2), 6b(b2), 6c(c2), 6d(d2), 7a(a2), and 7a(b2)). The hypocenter spread on the AA′ projection seems thicker due to conjugate ~N-S seismicity that cuts across the main ~ENE trend and from a minor tilt in the plane of hypocenters from the vertical to the NNW. Although the BB′ projections show narrow bands of earthquake swarms that can be interpreted as small-scale N-S features at depth, the AA′ projections and the epicenter maps continue to indicate a tight plane of hypocenters in the ~ENE-WSW direction. There are exceptions such as the ~N-S seismic swarm in April 1998 in TW-5 at the western end of the zone (Figures 6d(d2) and 6d(d3)). The ~N-S trending aftershocks from the 4 June 1998 Hengill earthquake also extend into the study area as seen in TW-6 (Figure 7a). As in the previous TWs, the BB′ projection for events in TW-6 shows some hypocenters aligning along small N-S features over the ~ENE plane (Figure 7a). The epicenter map for TW-7 shows an ~ENE trend intersected by two conjugate ~N-S features: one in the middle of the ~ENE trending aftershocks and the other to the east of their eastern terminus (Figure 7b). Again, the AA′ projection shows hypocenters mostly confined in the ~ENE direction, while the BB′ projection illustrates the dense and relatively even packing of hypocenters on the ~ENE-WSW plane (Figures 7b(b2) and 7b(b3)).

Figures 8 and 9 illustrate the evolution of events surrounding the 13 November earthquake. The mainshock originated near the intersection of hypocenters aligning in the ~ENE-WSW and ~N-S directions (Figure 9). The fact that Set 1 of foreshocks (24–48 hr before mainshock) occurred in the ~N-S direction followed by Set 2 of foreshocks (subsequent 24 hr) in the ~ENE-WSW to E-W direction (Figures 9c and S8) indicates slip on an ~N-S plane with normal-stress reduction in the ~E-W direction and subsequent activation. The progression of foreshocks over time indicates that the mainshock likely occurred on an ~ENE-WSW fault. This is further enforced by the prominent aftershock activity in this direction

immediately after the mainshock (Figure 9c and Movie S2). Mainshock relocations listed in Table S1 and plotted in Figure 9d place the event in the NW quadrant of the intersection between the conjugate seismicity. However, the exact location of the mainshock is ambiguous, as detailed here. It is reasonable to infer that the event might have nucleated at or close to the junction of the conjugate ~ENE-WSW and ~N-S faults. We assume that the mainshock's longitude is better constrained than its latitude (higher station coverage in the E-W direction; see example for latitude/longitude error estimates in Figure S7) and that it may be located on the western half of the ENE fault with reduced normal stress due to the foreshock activity. Set 1 foreshocks are also on the ENE fault, gradually breaking up the asperity leading to the mainshock. This ENE-WSW segment in Hjalli-Ölfus was likely triggered by the June 1998 Hengill earthquake. The seismic activity in Hengill was due to the minor intrusion event on a tectonically loaded region east of the Hengill volcano in the years 1994–1998 (Feigl et al., 2000; Sigmundsson et al., 1997) (Figure 2a). It is probable that dextral slip on the N-S faults in the Hengill region variably loaded the Hjalli-Ölfus plane. These south-propagating dextral faults from Hengill likely locked up part of the ENE-WSW plane (eastern side of ENE aligning epicenters) while easing up the other (reduced normal stress) (Figures 7a). The spread of hypocenters during the 13 November 1998 sequence fits well with this hypothesis as there was larger stress release west of the ~N-S inferred/proposed fault activated by the June 1998 Hengill event and comparatively lower seismicity to its east with gradual expansion in this direction with time. However, this requires computational validation and presents scope for future study of interactive stress behavior between Hengill and Ölfus.

Additionally, we compute the slips corresponding to a Mw 5.1 mainshock occurring on either the ~N-S or the ~ENE-WSW fault using the formula $M_0 = \mu AD$, where M_0 is the moment energy, μ is the rigidity modulus, A is the fault area, and D is the average slip. For an ~N-S rupture, Rognvaldsson et al. (1998) estimate a total slip of 17 cm based on a circular fracture model. From this study, we estimate that for an ~N-S rupture of length ~1.0 km (1 hr of aftershocks at the junction of conjugate faults; Figure 9c), maximum width ~4.0 km (from depth range 4–8 km), and rigidity (μ) 30 GPa, the average slip for a moment release of $M_0 = 5.43 \times 10^{16}$ N-m (Mw 5.1; GCMT) amounts to ~45 cm. For an ~N-S fault of length ~4 km (foreshock and aftershock spread in Figures 8 and 9b) and width of 4 km, the slip value turns out to be ~11 cm. Meanwhile, for an ~ENE-WSW rupture of length 6 km (first hour aftershock spread in Figure 9c) and width ~4 km, the slip value equals ~8 cm. If we assume a rupture length of 10 km (Figures 7b and 8b) following the aftershock area expansion over the subsequent hours and days, the slip is ~5 cm (Movie S2). The rupture area for a Mw 5.38 strike-slip event is ~39 km^2 with slip ~9–11 cm based on revised empirical earthquake source-scaling laws for events $5.38 \leq Mw \leq 8.70$ (Thingbaijam et al., 2017). The estimated slip values for both faults are comparable to the empirical slip values (although averages) obtained for a Mw 5.38 event. However, the occurrence of the larger proportion and magnitudes of aftershocks in the ~ENE direction and the agreement of slip estimates in this direction with average empirical values support the idea that the 13 November 1998 event likely ruptured along the ~ENE-WSW direction.

The only instance of similar ENE-WSW seismic activity in Hjalli-Ölfus after November 1998 was when the May 2008 earthquakes triggered increased low-magnitude seismic activity in west Ölfus, spanning less than 8-km depth (Brandsdóttir et al., 2010). The seismic depth estimates between 2- and 8-km depth from our study converges with this observation. Tomographic studies from South and West Iceland indicate an ~20- to 24-km-thick crust and an upper crust that follows a trend of increasing thickness from 4 km in the WVZ to 7 km in the eastern part of SISZ (Bjarnason, Menke, et al., 1993; Stefánsson et al., 1993; Tryggvason et al., 2002). Therefore, the slips from the 2008 doublet and the 1998 earthquake were most likely confined within the shallow brittle crust. Although geodetic studies show an increase in static stress and resulting seismicity in Hjalli-Ölfus from the 2008 earthquakes, no significant slip was observed on this segment (Decriem et al., 2010). Presumably, the Hjalli-Ölfus fault was either locked at seismogenic depths at the time or enough stress was released in the 1998 events so that the static stress change in 2008 was insufficient for further slip. Some authors ascribe the necessary weakening of the associated faults in the SISZ for release of large earthquakes to change in pore pressure due to magma dehydration in the asthenosphere and fluid movement into the lower crust (Stefánsson, 2011; Stefánsson et al., 2011). However, a tangible role of fluids here is still unclear, much like the interplay between sinistral shear along SISZ and magmatic/tectonic movement in Hengill.

6. Conclusions

The Hjalli-Ölfus seismic belt is a mixture of cross-cutting ~ENE-WSW and ~N-S faults, with most of its seismicity confined to the former than the latter. We see conjugate faulting on all scales, from a few 100 m to ~10 km, where slip on one fault seems to trigger slip on a conjugate neighbor. This trend partly mirrors those seen in RP and the rest of SISZ. Therefore, this study affirms the idea that the Hjalli-Ölfus segment potentially serves as a transition region between the two legs of the main plate boundary. The November 1998 Hjalli-Ölfus earthquake nucleated close to the junction of the ~ENE-WSW fault and a central throughgoing ~N-S fault. However, it likely ruptured along the ~ENE-WSW direction as suggested by the foreshock-aftershock spread, computed rupture area, and average slip. A lesser proportion of events occurred on two ~N-S lineaments, one cutting across the main ~ENE aftershock spread and the other ~1 km east of the ~ENE aftershock terminus. Most Hjalli-Ölfus events occur within 4- to 8-km depth, while the hypocenter distribution extending from Hengill is restricted to ~2–5 km. This indicates a thicker brittle crustal layer in western SISZ in comparison to the volcanic region in Hengill, as expected. The focal mechanisms of the foreshocks and aftershocks of the November 1998 event illustrate a mixture of strike-slip and oblique normal events. Foreshocks less than a day prior to the mainshock and the ensuing aftershocks follow an ~ENE-WSW alignment and are mostly strike-slip events with the most consistent nodal planes oriented in the said direction, indicating sinistral slip on a steeply dipping ~ENE-WSW fault. The subsequent paper to this study will analyze seismic data from July 1991 to December 1999 to identify spatiotemporal evolution of stress fields and faulting mechanisms in the Hjalli-Ölfus seismic belt.

Data Availability Statement

The relocated earthquake catalogs, station lists, and seismic velocity model used have all been uploaded to the Open Science Framework website following the AGU FAIR-data policy (https://osf.io/a58fv/?view_only=02c75823f6c24da98ca6adbab5543567). Details of the uploaded data can also be found in the supporting information submitted with the manuscript.

Acknowledgments

This study was part of the project titled "4D seismic of the South Iceland Seismic Zone: Strong earthquake forecasting" (152432-053) funded by the Icelandic Research Fund (IRF) (Rannís). The authors thank Felix Waldhauser for sharing a more recent version of the hypoDD routine, which was then modified for the purposes of this study, and for advice on fine-tuning the analyses. The authors thank Haukur Jóhannesson, Kristján Sæmundsson, Árni Hjartarson, Maryam Khodayar, Leó Kristjánsson, and Ágúst Guðmundsson for insightful discussions. The authors also thank Páll Einarsson and Bryndís Brandsdóttir for scientific discussion and for sharing seismic data from 1974 to 1987. The project facilitated the procurement of seismic data recorded by the SIL seismic network from the Icelandic Meteorological Office (IMO), and the raw version of this data can only be obtained directly from the agency.

References

Angelier, J., Bergerat, F., Bellou, M., & Homberg, C. (2004). Co-seismic strike–slip fault displacement determined from push-up structures: The Selsund Fault case, South Iceland. *Journal of Structural Geology*, *26*(4), 709–724. https://doi.org/10.1016/j.jsg.2003.07.006

Ármannsdóttir, S. (2008). Endurstaðsetning jarðskjálfta á Hengilssvæðinu 1. apríl 1955 út frá jarðskjálftaáhrifum: BS-these from University of Iceland (in Icelandic). http://hdl.handle.net/10802/4340

Arnadóttir, T. H., Jónsson, S., Pedersen, R., & Gudmundsson, G. B. (2003). Coulomb stress changes in the South Iceland Seismic Zone due to two large earthquakes in June 2000. *Geophysical Research Letters*, *30*(5), 1205. https://doi.org/10.1029/2002GL016495

Árnadóttir, T., Geirsson, H., & Einarsson, P. (2004). Coseismic stress changes and crustal deformation on the Reykjanes Peninsula due to triggered earthquakes on 17 June 2000. *Journal of Geophysical Research*, *109*, B09307. https://doi.org/10.1029/2004JB003130

Árnadóttir, T., Geirsson, H., & Jiang, W. (2008). Crustal deformation in Iceland: Plate spreading and earthquake deformation. *Jökull*, *58*, 59–74.

Árnadóttir, T., Haines, J., Geirsson, H., & Hreinsdóttir, S. (2018). A preseismic strain anomaly detected before *M* 6 earthquakes in the South Iceland Seismic Zone from GPS station velocities. *Journal of Geophysical Research: Solid Earth*, *123*, 11,091–11,111. https://doi.org/10.1029/2018JB016068

Árnadóttir, T., Hreinsdóttir, S., Gudmundsson, G., Einarsson, P., Heinert, M., & Völksen, C. (2001). Crustal deformation measured by GPS in the South Iceland Seismic Zone due to two large earthquakes in June 2000. *Geophysical Research Letters*, *28*, 4031–4033. https://doi.org/10.1029/2001GL013332

Árnadóttir, T., Jiang, W., Feigl, K. L., Geirsson, H., & Sturkell, E. (2006). Kinematic models of plate boundary deformation in Southwest Iceland derived from GPS observations. *Journal of Geophysical Research*, *111*, B07402. https://doi.org/10.1029/2005JB003907

Bergerat, F., & Angelier, J. (2008). Immature and mature transform zones near a hot spot: The South Iceland Seismic Zone and the Tjörnes Fracture Zone (Iceland). *Tectonophysics*, *447*(1–4), 142–154. https://doi.org/10.1016/j.tecto.2006.05.046

Bjarnason, I. T., Menke, W., Flóvenz, Ó. G., & Caress, D. (1993). Tomographic image of the mid-Atlantic plate boundary in southwestern Iceland. *Journal of Geophysical Research*, *98*(B4), 6607–6622. https://doi.org/10.1029/92JB02412

Bjarnason, I. T., Cowie, P., Anders, M. H., Seeber, L., & Scholz, C. H. (1993). The 1912 Iceland earthquake rupture: Growth and development of a nascent transform system. *Bulletin of the Seismological Society of America*, *83*(2), 416–435.

Bjarnason, I. T., & Einarsson, P. (1991). Source mechanism of the 1987 Vatnafjöll earthquake in South Iceland. *Journal of Geophysical Research*, *96*(B3), 4313–4324. https://doi.org/10.1029/90JB00831

Bjarnason, I. Th. & Thorbjarnardóttir, B. S. (2019). Absolute and relative location errors in double-difference relative earthquake locations in Southwest Iceland. EGU General Assembly Conference Abstracts, p.16,458. https://ui.adsabs.harvard.edu/abs/2019EGUGA..2116458B

Björnsson, S. (1976). Earthquakes in Iceland (in Icelandic, with English abstract). *Náttúrufrædingurinn*, *45*(2), 110–133. https://hdl.handle.net/20.500.11815/1323

Björnsson, S., Einarsson, P., Tulinius, H., & Hjartardóttir, Á. R. (2018). Seismicity of the Reykjanes Peninsula 1971–1976. *Journal of Volcanology and Geothermal Research*, *391*, 106369. https://doi.org/10.1016/j.jvolgeores.2018.04.026

Brander, J. L., Mason, R. G., & Calvert, R. W. (1976). Precise distance measurements in Iceland. *Tectonophysics*, *31*(3–4), 193–206. https://doi.org/10.1016/0040-1951(76)90119-0

Brandsdóttir, B., Parsons, M., White, R. S., Gudmundsson, O., Drew, J., & Thorbjarnadóttir, B. S. (2010). The May 29, 2008 earthquake aftershock sequence within the South Iceland Seismic Zone: Fault locations and source parameters of aftershocks. *Jökull: journal of the glaciological and geological societies of Iceland*, *60*, 23–46.

Clifton, A. E., & Einarsson, P. (2005). Styles of surface rupture accompanying the June 17 and 21, 2000 earthquakes in the South Iceland Seismic Zone. *Tectonophysics*, *396*, 141–159. https://doi.org/10.1016/j.tecto.2004.11.007

Clifton, A. E., & Schlische, R. W. (2003). Fracture populations on the Reykjanes Peninsula, Iceland: Comparison with experimental clay models of oblique rifting. *Journal of Geophysical Research*, *108*(B2), 2074. https://doi.org/10.1029/2001JB000635

Davis, G. H., Bump, A. P., Garcia, P. E., & Ahlgren, S. G. (2000). Conjugate Riedel deformation band shear zones. *Journal of Structural Geology*, *22*(2), 169–190. https://doi.org/10.1016/S0191-8141(99)00140-6

Decriem, J., Árnadóttir, T., Hooper, A., Geirsson, H., Sigmundsson, F., Keiding, M., et al. (2010). The 2008 May 29 earthquake doublet in SW Iceland. *Geophysical Journal International*, *181*(2), 1128–1146. https://doi.org/10.1111/j.1365-246X.2010.04565.x

DeMets, C., Gordon, R. G., & Argus, D. F. (2010). Geologically current plate motions. *Geophysical Journal International*, *181*(1), 1–80. https://doi.org/10.1111/j.1365-246X.2009.04491.x

Einarsson, P. (1991). Earthquakes and present-day tectonism in Iceland. *Tectonophysics*, *189*, 261–279. https://doi.org/10.1016/0040-1951(91)90501-I

Einarsson, P. (2008). Plate boundaries, rifts and transforms in Iceland. *Jökull*, *58*, 35–58.

Einarsson, P., & Björnsson, S. (1979). Earthquakes in Iceland. *Jökull*, *29*, 37–43.

Einarsson, P., & Björnsson, S. (1987). Jardskjalftamaelingar á Raunvísindastofnun Háskólans. Í hlutarins edli: Festschrift for Thorbjörn Sigurgeirsson. Menningarsjodur, 251–278.

Einarsson, P., Björnsson, S., Foulger, G. R., Stefánsson, R., & Skaftadóttir, T. (1981). Seismicity pattern in the South Iceland Seismic Zone. In D. Simpson, & P. G. Richards (Eds.), *Earthquake prediction—An international review*, *American Geophysical Union, Maurice Ewing Series* (Vol. 4, pp. 141–151). USA: American Geophysical Union (AGU).

Einarsson, P., & Eiríksson, J. (1982). Earthquake fractures in the districts land and Rangárvellir in the South Iceland Seismic Zone. *Jökull*, *32*, 113–120.

Erlendsson, P., & Einarsson, P. (1996). The Hvalhnúkur Fault, a strike-slip fault mapped within the Reykjanes Peninsula oblique rift, Iceland. In B. Thorkelsson (Ed.), *Seismology in Europe* (pp. 498–504). Icelandic Meteorological Office, Reykjavík, Iceland: European Seismological Commission.

Feigl, K. L., Gasperi, J., Sigmundsson, F., & Rigo, A. (2000). Crustal deformation near Hengill volcano, Iceland, 1993–1998: Coupling between magmatic activity and faulting inferred from elastic modeling of satellite radar interferograms. *Journal of Geophysical Research*, *105*, 25,655–25,670. https://doi.org/10.1029/2000JB900209

Foulger, G. R. (1988). Hengill triple junction, SW Iceland 1. Tectonic structure and the spatial and temporal distribution of local earthquakes. *Journal of Geophysical Research*, *93*(B11), 13,493–13,506. https://doi.org/10.1029/JB093iB11p13493

Gudmundsson, A. (2007). Infrastructure and evolution of ocean-ridge discontinuities in Iceland. *Journal of Geodynamics*, *43*(1), 6–29. https://doi.org/10.1016/j.jog.2006.09.002

Gudmundsson, A., & Brynjolfsson, S. (1993). Overlapping rift-zone segments and the evolution of the South Iceland Seismic Zone. *Geophysical Research Letters*, *20*(18), 1903–1906. https://doi.org/10.1029/93GL01888

Gudmundsson, A. (2017). *The glorious geology of Iceland's golden circle*. Cham, Switzerland: Springer-Nature. https://link.springer.com/book/10.1007%2F978-3-319-55152-4

Gutenberg, B. & Richter, C. F. (1954). Seismicity of the Earth: Princeton, NJ.

Halldórsson, P., Björnsson, S., Brandsdóttir, B., Sólnes, J., Stefánsson, R., & Bessason, B. (2013). *Earthquakes in Iceland*, *Natural hazard in Iceland, volcanic eruptions and earthquakes*. Iceland: University of Iceland Press and Iceland Catastrophe Insurance.

Hensch, M., Lund, B., Árnadóttir, T., & Brandsdóttir, B. (2016). Temporal stress changes associated with the 2008 May 29 MW 6 earthquake doublet in the western South Iceland Seismic Zone. *Geophysical Journal International*, *204*(1), 544–554. https://doi.org/10.1093/gji/ggv465

Hjaltadóttir, S. (2009). Use of relatively located microearthquakes to map fault patterns and estimate the thickness of the brittle crust in Southwest Iceland. MS-thesis. University of Iceland (104 pp).

Hreinsdóttir, S., Árnadóttir, T., Decriem, J., Geirsson, H., Tryggvason, A., Bennett, R. A., & LaFemina, P. (2009). A complex earthquake sequence captured by the continuous GPS network in SW Iceland. *Geophysical Research Letters*, *36*, L12309. https://doi.org/10.1029/2009GL038391

Hreinsdóttir, S., Einarsson, P., & Sigmundsson, F. (2001). Crustal deformation at the oblique spreading Reykjanes Peninsula, SW Iceland: GPS measurements from 1993 to 1998. *Journal of Geophysical Research*, *106*(B7), 13,803–13,816. https://doi.org/10.1029/2001JB000428

Icelandic Meteorological Office (2017). Preliminary analysed data by the SIL seismic monitoring group of the Icelandic Meteorological Office, accessed January, 2017.

Jakobsdóttir, S. S. (2008). Seismicity in Iceland: 1994–2007. *Jökull*, *58*, 75–100.

Karson, J. A. (2017). The Iceland plate boundary zone: Propagating rifts, migrating transforms, and rift-parallel strike-slip faults. *Geochemistry, Geophysics, Geosystems*, *18*, 4043–4054. https://doi.org/10.1002/2017GC007045

Karson, J. A., Brandsdóttir, B., Einarsson, P., Sæmundsson, K., Farrell, J. A., & Horst, A. J. (2019). Evolution of migrating transform faults in anisotropic oceanic crust: Examples from Iceland. *Canadian Journal of Earth Sciences*, *56*(12), 1297–1308. https://doi.org/10.1139/cjes-2018-0260

Karson, J. A., Farrell, J. A., Chutas, L. A., Nanfito, A. F., Proett, J. A., Runnals, K. T., & Sæmundsson, K. (2018). Rift-parallel strike-slip faulting near the Iceland Plate Boundary Zone: Implications for propagating rifts. *Tectonics*, *37*, 4567–4594. https://doi.org/10.1029/2018TC005206

Keiding, M., Árnadóttir, T., Sturkell, E., Geirsson, H., & Lund, B. (2008). Strain accumulation along an oblique plate boundary: The Reykjanes Peninsula, Southwest Iceland. *Geophysical Journal International*, *172*(2), 861–872. https://doi.org/10.1111/j.1365-246X.2007.03655.x

Keiding, M., Lund, B., & Árnadóttir, T. (2009). Earthquakes, stress and strain along an oblique plate boundary: The Reykjanes Peninsula, Southwest Iceland. *Journal of Geophysical Research*, *114*, B09306. https://doi.org/10.1029/2008JB006253

Khodayar, M., Björnsson, S., Guðnason, E. Á., Níelsson, S., Axelsson, G., & Hickson, C. (2018). Tectonic control of the Reykjanes geothermal field in the oblique rift of SW Iceland: From regional to reservoir scales. *Open Journal of Geology*, *8*(03), 333. https://doi.org/10.4236/ojg.2018.83021

Khodayar, M., Björnsson, S., Víkingsson, S., & Jónsdóttir, G. (2020). Unstable rifts, a leaky transform zone and a microplate: Analogues from South Iceland. *Open Journal of Geology*, *10*, 317–367. https://doi.org/10.4236/ojg.2020.104017

Khodayar, M., & Franzson, H. (2007). Fracture pattern of Thjórsárdalur central volcano with respect to rift-jump and a migrating transform zone in South Iceland. *Journal of Structural Geology*, *29*(5), 898–912. https://doi.org/10.1016/j.jsg.2006.11.007

LaFemina, P. C., Dixon, T. H., Malservisi, R., Árnadóttir, T., Sturkell, E., Sigmundsson, F., & Einarsson, P. (2005). Strain partitioning and accumulation in a propagating ridge system: Geodetic GPS measurements in South Iceland. *Journal of Geophysical Research*, *110*, B11405. https://doi.org/10.1029/2005JB003675

Porter, C., Morin, P., Howat, I., Noh, M., Bates, B., Peterman, K., et al. (2018). "ArcticDEM", Harvard Dataverse, V1, [Last 25 October 2019].

Rognvaldsson, S. T., Árnadottir, P., Águstsson, K., Skaftadottir, P., Guomundsson, G. B., Bjornsson, G., et al. (1998). Skjalftahrina f Olfusi f november 1998. Technical Report (in Icelandic with English summary).

Roth, F. (2004). Stress changes modelled for the sequence of strong earthquakes in the South Iceland Seismic Zone since 1706. In Geodetic and geophysical effects associated with seismic and volcanic hazards (1305–1327). Birkhäuser, Basel. https://doi.org/10.1007/978-3-0348-7897-5_2

Sigmundsson, F., Einarsson, P., Hjartardóttir, Á. R., Drouin, V., Jónsdóttir, K., Árnadóttir, T., et al. (2018). Geodynamics of Iceland and the signatures of plate spreading. *Journal of Volcanology and Geothermal Research*, *391*, 106436. https://doi.org/10.1016/j.jvolgeores.2018.08.014

Sigmundsson, F., Einarsson, P., Rögnvaldsson, S. T., Foulger, G. R., Hodgkinson, K. M., & Thorbergsson, G. (1997). The 1994–1995 seismicity and deformation at the Hengill triple junction, Iceland: Triggering of earthquakes by minor magma injection in a zone of horizontal shear stress. *Journal of Geophysical Research*, *102*(B7), 15,151–15,161. https://doi.org/10.1029/97JB00892

Stefánsson, R. (2011). *Advances in earthquake prediction, research and risk mitigation* (p. 271). Springer-Verlag, Berlin and Heidelberg: association with PRAXIS Publishing in UK.

Stefánsson, R., Bodvarsson, R., Slunga, R., Einarsson, P., Jakobsdottir, S., Bungum, H., et al. (1993). Earthquake prediction research in the South Iceland seismic zone and the SIL project. *Bulletin of the Seismological Society of America*, *83*, 696–716.

Stefánsson, R., Bonafede, M., & Gudmundsson, G. B. (2011). Earthquake-prediction research and the earthquakes of 2000 in the South Iceland Seismic Zone. *Bulletin of the Seismological Society of America*, *101*(4), 1590–1617. https://doi.org/10.1785/0120090093

Stefánsson, R., Guðmundsson, G. B and Halldórsson, P. (2000). The two large earthquakes in the South Iceland seismic zone on June 17 and 21, 2000. Report VI-GOOOlO-JA04, Icelandic Meteorology Office.

Stefánsson, R., & Halldórsson, P. (1988). Strain build-up and strain release in the South Iceland seismic zone. *Tectonophysics*, *152*(3-4), 267–276. https://doi.org/10.1016/0040-1951(88)90052-2

Steigerwald, L., Einarsson, P., & Hjartardóttir, Á. R. (2018). Fault kinematics at the Hengill Triple Junction, SW-Iceland, derived from surface fracture pattern. *Journal of Volcanology and Geothermal Research*, *391*, 106439. https://doi.org/10.1016/j.jvolgeores.2018.08.017

Taylor, B., Crook, K., & Sinton, J. (1994). Extensional transform zones and oblique spreading centers. *Journal of Geophysical Research*, *99*(B10), 19,707–19,718. https://doi.org/10.1029/94JB01662

Thingbaijam, K. K. S., Martin Mai, P., & Goda, K. (2017). New empirical earthquake source-scaling laws. *Bulletin of the Seismological Society of America*, *107*(5), 2225–2246. https://doi.org/10.1785/0120170017

Thorbjarnardóttir, B. S., Bjarnason, I. T. & Stefánsson, R. (2018). Seismotectonics and triggered earthquakes in the Geysir Area in Iceland. In EGU general assembly conference abstracts (Vol. 20, p. 15567). https://ui.adsabs.harvard.edu/#abs/2018EGUGA..2015567T/abstract

Tryggvason, A., Rögnvaldsson, S. T., & Flóvenz, O. G. (2002). Three-dimensional imaging of the *P*- and *S*-wave velocity structure and earthquake locations beneath Southwest Iceland. *Geophysical Journal International*, *151*(3), 848–866. https://doi.org/10.1046/j.1365-246X.2002.01812.x

Tryggvason, E. (1954). Jarðskjálftar á Íslandi árið 1953 (in Icelandic, with English abstract). *Náttúrufræðingurinn*, *24*(1), 1–6. https://hdl.handle.net/20.500.11815/1325

Tryggvason, E. (1956). Jarðskjálftar árin 1954 og 1955 (in Icelandic, with English abstract). *Nátturufr*, *26*(2), 77–86. https://hdl.handle.net/20.500.11815/1326

Tryggvason, E. (1973). Seismicity, earthquake swarms, and plate boundaries in the Iceland region. *Bulletin of the Seismological Society of America*, *63*(4), 1327–1348.

Vogfjörd, K. S., Hjaltadóttir, S., & Slunga, R. (2005). Volcano-tectonic interaction in the Hengill region, Iceland during 1993–1998. In *Geophys. Res. Abstracts* (Vol. 7, p. 09947). Vienna, Austria: EGU General Assembly.

Waldhauser, F. (2001). hypoDD—A program to compute double-difference hypocenter locations.

Waldhauser, F., & Ellsworth, W. L. (2000). A double-difference earthquake location algorithm: Method and application to the northern Hayward fault, California. *Bulletin of the Seismological Society of America*, *90*(6), 1353–1368. https://doi.org/10.1785/0120000006